Supplementary Material

Table of Contents:

Supplementary Table 1. Methylation-Specific PCR Primers

DMR	Status of DNA	Forward Primer	Reverse Primer
DMR 8	Methylated	TTTTATGTTTATGTCGGGGTAGC	AAAAAACCCGAAAACAATAATACG
	Unmethylated	TTTATGTTTATGTTGGGGTAGTGG	AAAAACCCAAAAACAATAATACAAA
DMR 9	Methylated	TTTCGTGGTTTTAATATAGGGTTTC	CTAAACTTACCTAAAATTTCCCGAC
	Unmethylated	TTTGTGGTTTTAATATAGGGTTTTG	CTAAACTTACCTAAAATTTCCCAAC

Supplementary Table 2. qPCR Primers

| Gene	Forward Primer	Reverse Primer	Annealing Temp
RPL13	CCTGGAGGAGAAGAGGAAAGAGA	TTGAGGACCTCTGTTATTTGTC	60°C
HPRT	TGACACTGGCAAAACAATGCA	GGTCCTTTTCACCAGCAAGCT	60°C
ACTB	GCCCTGAGGCACTCTTCCA	CGGATGTCCACGTCACACTTC	60°C
HOXA5	GCACATAAGTCATGACAACATAG	CAGTACTTAAACGCTCAGATAC	60°C

Supplementary Figure 1A. EPIC Array and MSP methylation levels in CKD cases and healthy controls. A, D: DMR plots for DMR 8 and 9 respectively, showing the levels of methylation across the region of DMR. Pink lines show the methylation of the control samples, and green lines show the methylation of the CKD samples. B, E: EPIC Array methylation levels for probes the cg08373003 and cg22827250 captured by the MSP primers for DMRs 8 and 9 respectively, C, F: Methylation values as generated by the MSP reactions.
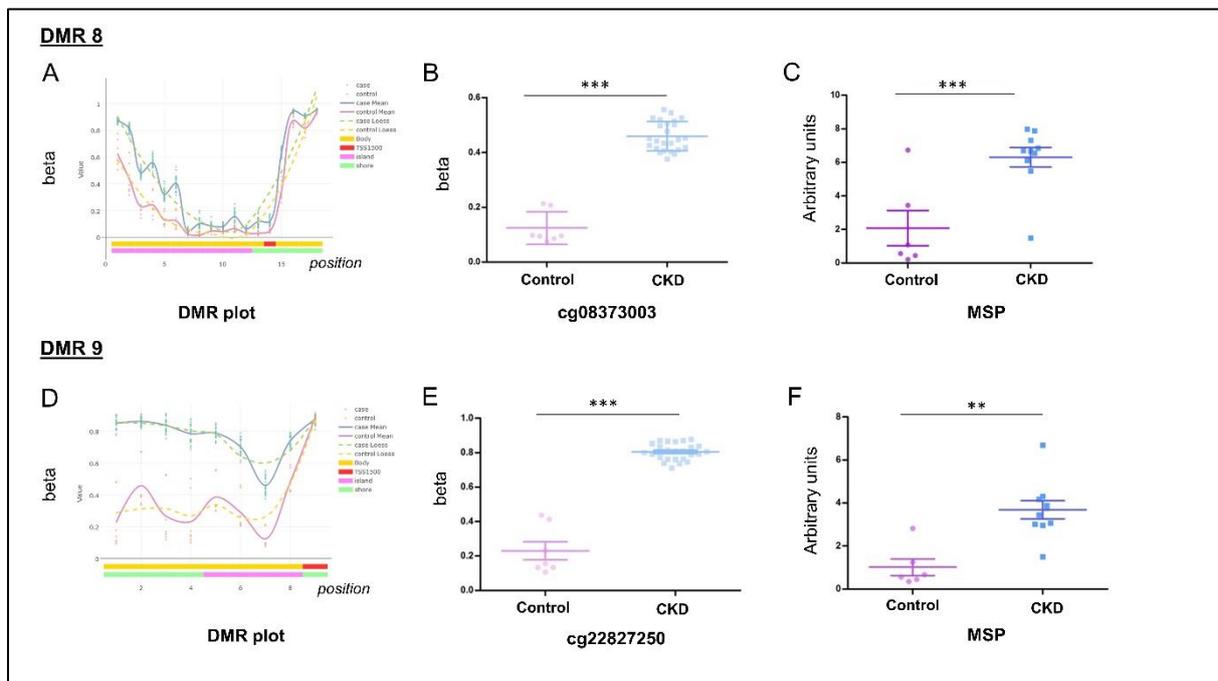
Supplementary Figure 1B. MSP analysis, EPIC array and MSP methylation levels in CKD cases and healthy controls in DMRs 102 and 125. A, E: Correlation analysis of methylation using MSP (y axis) and EPIC array methylation (x axis). B, F: DMR plots for DMR 102 and 125 respectively, showing the levels of methylation across the region of DMR. Pink lines show the methylation of the control samples, and green lines show the methylation of the CKD samples. C, G: EPIC Array methylation levels for the probes cg15793329 and cg13027595 captured by the MSP primer for DMR 102 and 125 respectively. D, H: Methylation values as generated by the MSP reactions.
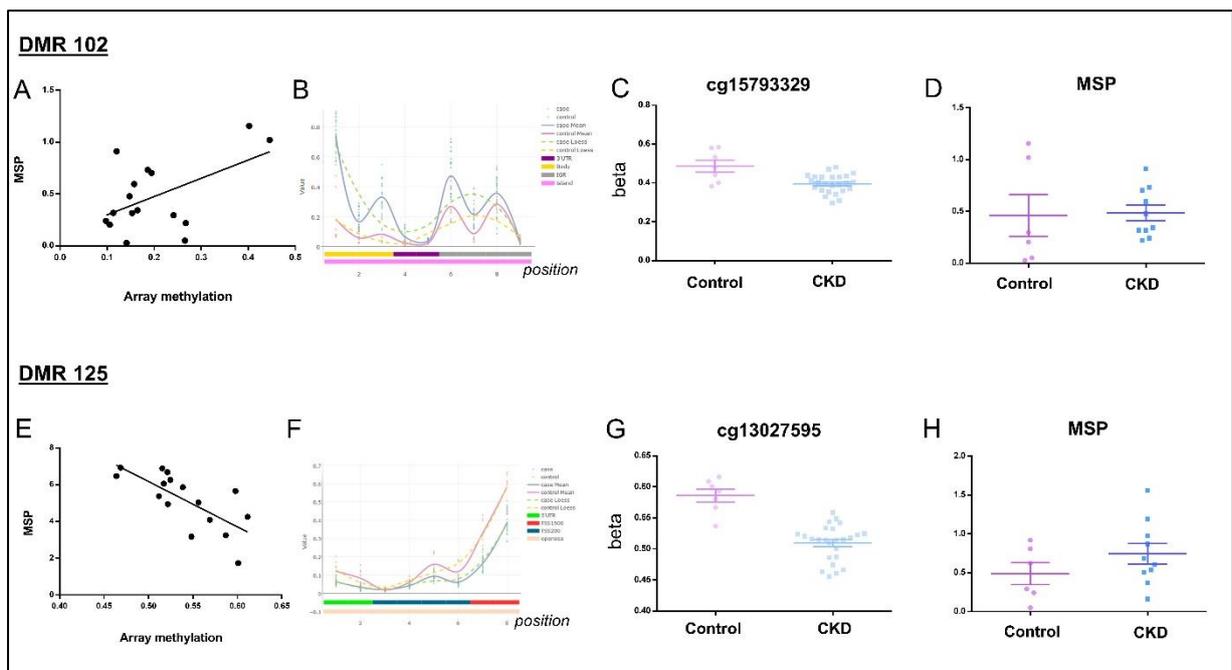
Supplementary Figure 2. Selected genes and the effect of differential methylation on DNA expression. A. Table with the genes and selection criteria. B. Gene expression of *HAND2* and correlation with the methylation values of DMR 7. C. Map showing the location of DMR 7, marked in red circle, in relation to *HAND2* and *HAND2-AS1*. Images adapted from UCSC Genome browser. D. Expression of *HAND2-AS1* in CKD and controls and the correlation of expression with methylation values of DMR 7. E-H. Gene expression of *HLX, SLC41A3, SVIL, FMOD* genes and correlation with the EPIC array methylation values. r = correlation coefficient.
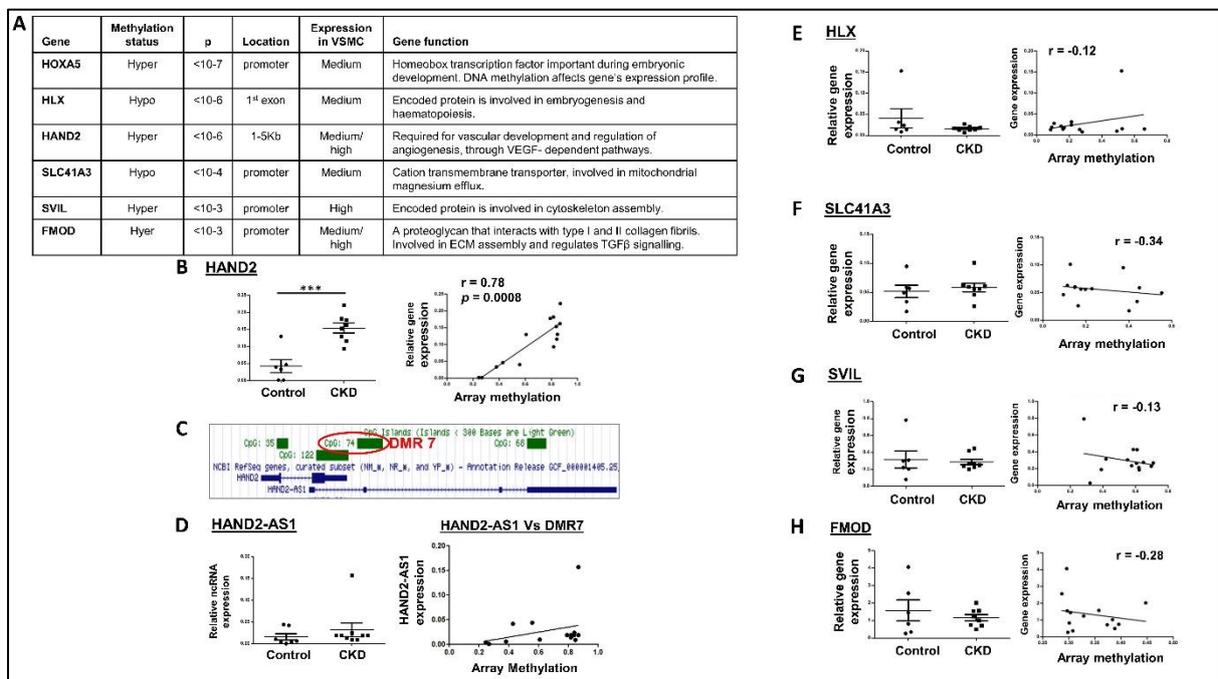
Supplementary Figure 3. Association of DNA methylation with protein and gene expression. A. Representative images of epigastric arteries of CKD (N=4) and healthy subjects (N=4) stained with a HOXA5 antibody, and quantification of staining using ImageJ. Insert: IgG Isotype control. B. Normalized gene expression of *HOXA5* in CKD subjects and healthy donors. C. Correlation analysis of gene (y axis) and protein expression (X axis) as assessed by qPCR and immunohistochemistry, respectively. The p-value and the r correlation coefficient are given for the Spearman correlation analysis.
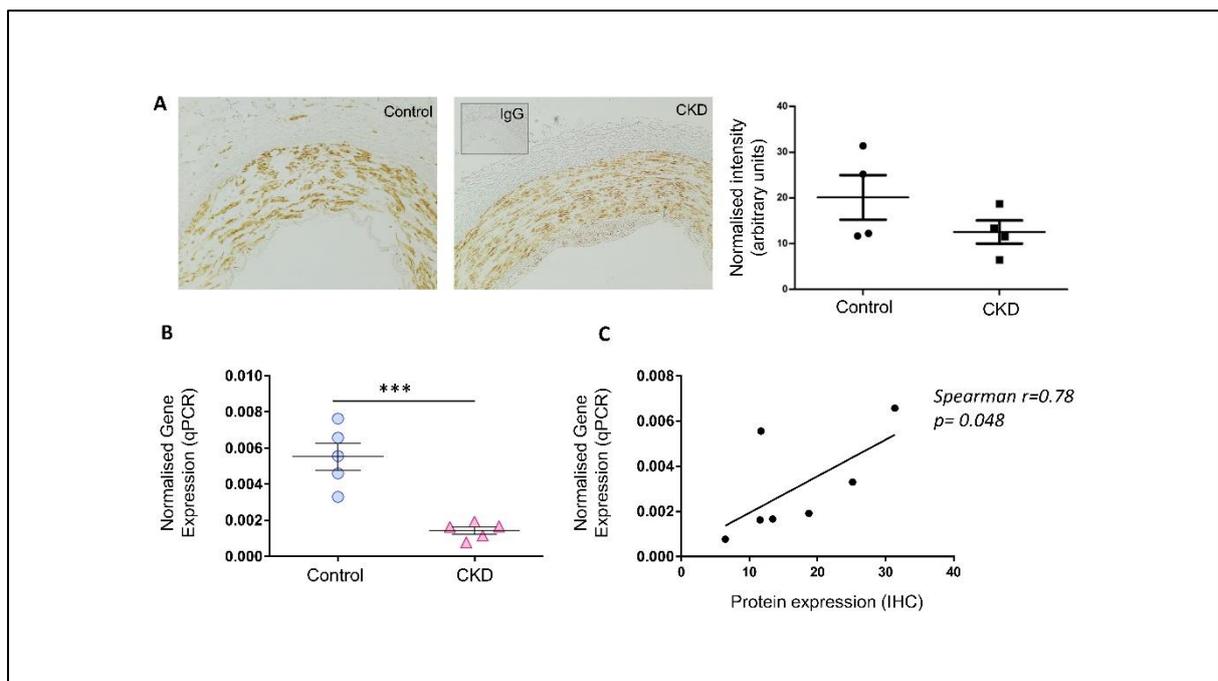
Supplementary Figure 4. SVD and QQ plots before and after ComBat analysis. The SVD analysis is shown as a heatmap of all the components of variation that have been included in the analysis. After the use ComBat and the removal of technical variation the p-values are slightly inflated as shown in the QQ plot of observed (y axis) and expected (x axis) values. Any biological variation was mostly associated with the presence of the disease (Sample_Group: case/control), as this was consistently highly associated with PC1 during SVD analysis.
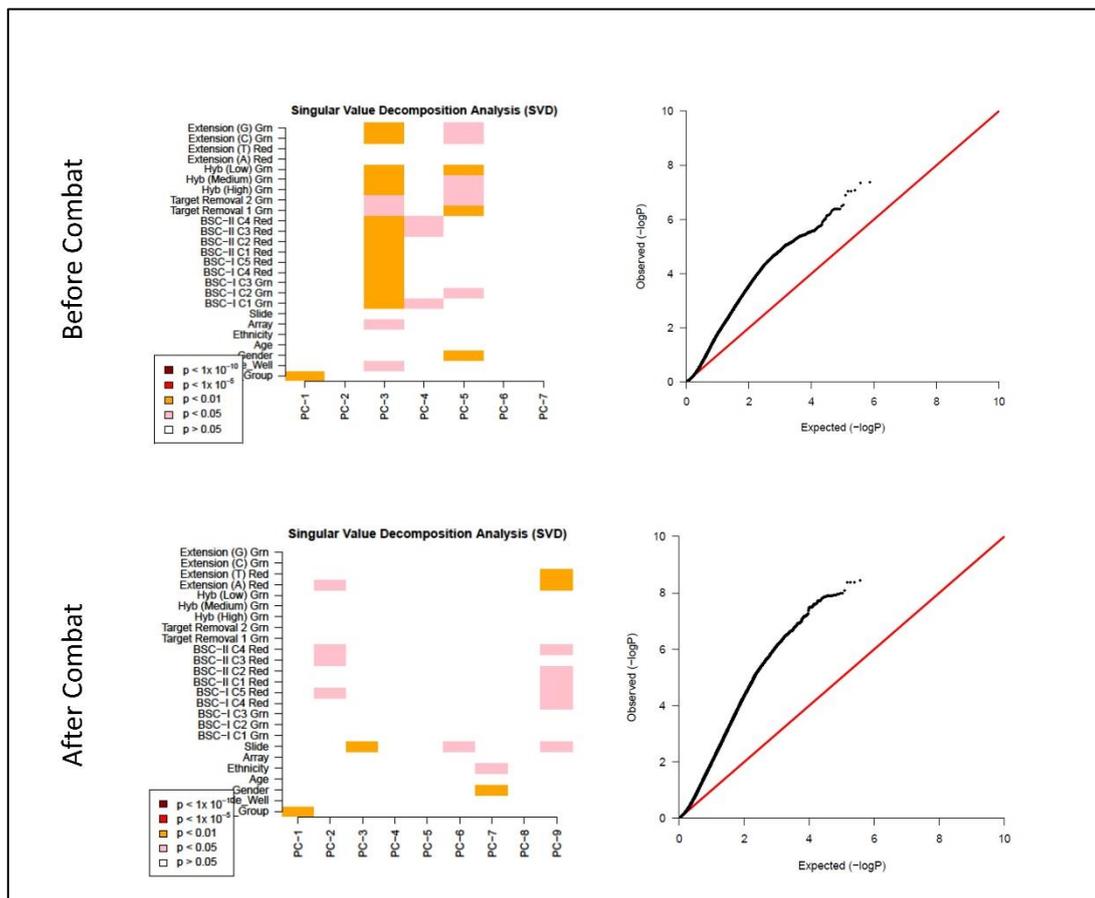
Supplementary Figure 5. EpiDISH Analysis to infer cell-type fractions from DNAm profiles of heterogeneous tissues. A beta value matrix with the beta values of all probes used in this study for each sample was used, and the cell type fraction was inferred using Robust Partial Correlations-RPC method (Teschendorff et al. 2017). Fractions of immune cell populations (B cell, Natural killer cells, CD4 T cells, Monocytes, Neutrophils, and Eosinophils) were poor, while fibroblasts, the cell type most similar to the vascular smooth muscle cells-our source of tissue, was the most abundant cell type.
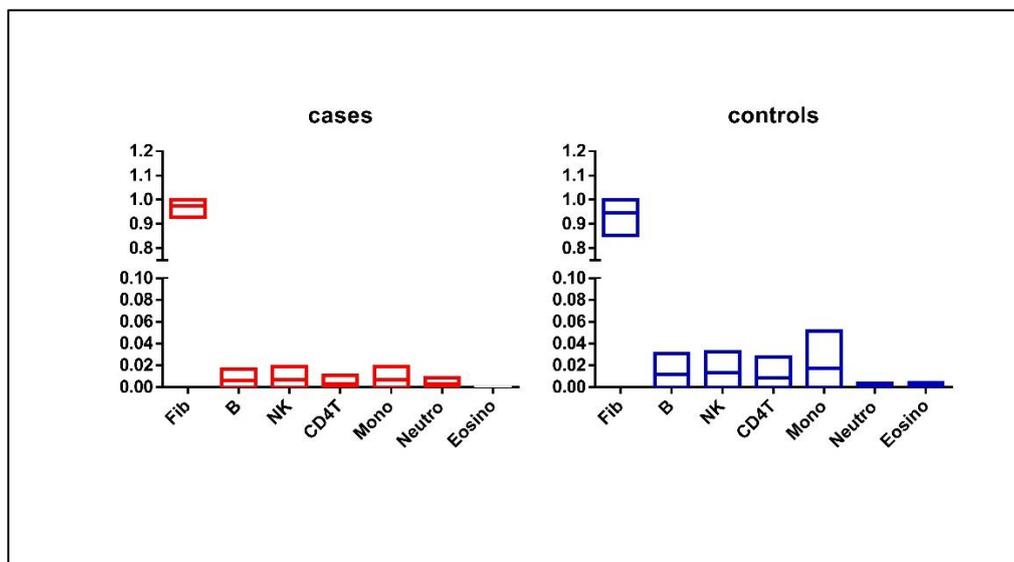
Supplementary Figure 6. Post-hoc power calculation using pwrEWAS. Given the size of our study cohort (32 samples), we have ~65% power to detect differences up to 20% in CpG-specific methylation across a hypothetical set of 10000 CpGs, and >80% power to detect differences up to 50% using the EPIC array (~750000 loci tested after filtering-out). This estimation is based on a tissue quite different to our source of DNA (adult PBMCs).